3D Printed Soil Analogs for Modeling of Coarse-Grained Soil Behavior

Sheikh Sharif Ahmed[1] and Alejandro Martinez, Ph.D.[2]

[1]Graduate Student, Dept. of Civil and Environmental Engineering, Univ. of California, Davis, Davis, CA. E-mail: ssah@ucdavis.edu
[2]Assistant Professor, Dept. of Civil and Environmental Engineering, Univ. of California, Davis, Davis, CA. E-mail: amart@ucdavis.edu

ABSTRACT

This paper presents the prospect of 3D printing technology to generate artificial soil analogs with the goal of modeling the mechanical behavior of coarse-grained soils. 3D X-ray CT scans of natural angular and rounded sand particles have been used to generate angular and rounded particle analogs using the polyjet 3D printing technology. A comparison of the scanned natural sand particles and the 3D printed particles demonstrates the ability of 3D printing technology to reproduce the shape and size of the sand particles. The results of oedometer compression tests on the angular and rounded natural and 3D printed particles are used to demonstrate the effect of constituent material (i.e. quartz versus polymer) stiffness on the measured soil compressibility and investigate the normalization of the response using the Hertz contact theory. The results provided in this paper also include comparison of the small-strain moduli–mean effective stress relationship obtained for the natural and 3D printed soils. This paper illustrates the potential use of 3D printed analogs to model the mechanical behavior of coarse-grained soils and identifies future research needs for implementation of the proposed normalization scheme within the critical state soil mechanics framework.

INTRODUCTION

Additive manufacturing technology is rapidly advancing. Modern 3D printers come in a wide spectrum of precision, capabilities and cost. Large-scale and more specialized 3D printers can print materials such as metals, ceramics, and polymers, and some of them can mix polymeric materials on demand to change their mechanical properties (e.g. Jiménez et al. 2019). More economic desktop 3D printers are typically constrained to printing polymeric materials; however, even these printers can achieve a precision of 10 to 30 μm. This rapid advancement in the technology is establishing 3D printers as a conventional tool in most engineering and science research laboratories (e.g. Tofail et al. 2018).

The mechanical behavior of coarse-grained soils is governed by the interactions at the contacts between discrete particles. The normal and shear deformation of inter-particle contacts are controlled by several particle properties such as shape, size, surface roughness and stiffness of their constituent materials. Additive manufacturing technology offers the ability to generate artificial soil analogs with independent control of particle properties. Testing with those analogs may provide more detailed insight on the effect of individual particle properties on the behavior of soils as compared to testing natural soils which simultaneously vary in several properties.

The research presented herein explores the feasibility of 3D printed soil analogs to model the behavior of coarse-grained soils. A representative number of angular and rounded natural sand particles were scanned using X-ray CT scanner and printed using a 3D printer. A comparative study of shape parameters (i.e. roundness and sphericity) for natural and 3D printed particles is performed. A normalization scheme based on Hertz contact theory is used to examine the 1D

compression stress–void ratio response of both natural particles and 3D printed analogs. Also, shear wave velocities and small-strain moduli of natural particles and 3D printed analog particles, obtained using the bender element test, are compared.

BACKGROUND

Elastic and Elastoplastic Contact Response: Hertz contact theory describes the normal force-displacement behavior of two elastic spheres in contact. The contact displacement and stress are functions of the normal contact force, radii of curvatures, modulus of elasticity, and Poisson's ratio. According to Hertz theory, if two elastic spheres of radii R_1 and R_2 are pressed into contact with a normal force F, the contact deformation, δ, is:

$$\delta = \left(\frac{9}{16} \frac{F^2}{RE^{*2}} \right)^{1/3} \quad (1)$$

where, R is the effective radius of curvature expressed as $1/R = 1/R_1 + 1/R_2$; and, E^* is the effective Young's modulus defined as $1/E^* = (1-\nu_1^2)/E_1 + (1-\nu_2^2)/E_2$, where R_1 and R_2 are the radii, E_1 and E_2 are the Young's moduli and ν_1 and ν_2 are the Poisson's ratios of the two bodies.

Hertz theory assumes elastic response between the bodies. However, most materials can exhibit yielding at the contact. Prior research has shown that the normal force–displacement response of two spherical particles usually follows the behavior predicted by Hertz theory within a certain force interval. For instance, Antonyuk et al. (2005) describes four stages of the particles tested in inter-platen compression, as shown in Figure 1. The response follows the four stages: i) plastic deformation of micro-asperities on the contact surface, ii) elastic deformation predicted by Hertz theory, iii) elastoplastic deformation, and iv) breakage.

Similar initial ductile response due to deformation of micro-asperities has been reported by Cavarretta et al. (2010), who observed the continuation of ductile response (stage I in Figure 1) until the contact normal force F exceeds given threshold force. The threshold force is dependent on the contact surface roughness, curvatures of the surfaces at the contact point, and Young's modulus of the bodies in contact (Greenwood and Tripp 1964)(Greenwood and Tripp 1967). Once F exceeds the threshold load, the force–displacement response is elastic and follows Hertz theory (stage II in Figure 1). Followed by stage II, the plastic yielding at the particle contact initiates and deviation from Hertz prediction is observed in stage III. At stage IV, the particle begins to break apart.

Research on Particle Contact Response: A number of authors have conducted particle-particle and single particle crushing tests on different materials to identify the parameters affecting the contact behavior. Several studies reported that the force–displacement behavior undergoes a transition from approximately linear behavior at lower forces to Hertzian behavior at higher force levels (e.g. Cole and Peters 2007, Cavarretta et al. 2010). Cavarretta et al. (2010) concluded that the threshold force at which Hertzian behavior takes over is dependent on particle size, roundness, surface roughness and the Young's modulus, and proposed a new particle-scale failure criterion. Also, other researchers have indicated the importance of particle shape over surface roughness (Nadimi and Fonseca 2017), and of initial particle morphology, heterogeneity and mineralogy (Zhao et al. 2015) on contact behavior. In addition, some authors (e.g. Senetakis et al. 2013) observed that particles with smaller mean surface roughness show a considerably higher initial tangential stiffness compared to particles with higher mean roughness.

Previous Studies on 3D Printed Soil Analogs: In recent years, several researchers have reported 3D printing of particles of different sizes and shapes. For example, Miskin and Jaeger

(2013) used an evolutionary algorithm to find the connection between particle shape and mechanical response of granular materials and performed triaxial tests on assembly of 3D printed spheres to compare them with molecular dynamics simulations. Athanassiadis et al. (2014) conducted triaxial tests on assemblies of 3D printed particles of different shapes and expressed the dependence of assembly stiffness on confining pressure by a power law ($E \propto \sigma_{con}^{n}$), where the exponent captures the shape dependence. Hanaor et al. (2016) performed triaxial tests on 3D printed particles of different shapes and sizes and demonstrated that 3D printed particle analogs can qualitatively reproduce soil behavior, including the effect of particle shape. Matsumura et al. (2017) reproduced bonded gravel specimen by means of X-ray imaging and 3D printing and performed triaxial tests on the 3D printed specimens. They reported the observation of both stress-level dependency and volumetric dilatancy typical of frictional granular materials during triaxial compression testing. Gupta et al. (2018) presented a reproducible and open-source test prototype consisting of five steps that utilizes 3D printing technology to generate multiscale data to support the calibration and validation of discrete element models (DEM) for granular materials. Adamidis et al. (2019) reproduced 3D printed analogs of Hostun sand using polyjet technology with three different scaling factors. Comparing the results obtained from both Hostun sand and 3D printed analogs, they concluded that, 3D printed particles can replicate well the particle morphology, and aspects of hydraulic conductivity and shear response of natural sand.

Kittu et al. (2019) performed particle characterization (e.g. Young's modulus, hardness, Poisson's ratio, inter-particle friction angle, and surface roughness) of 3D printed spheres of two different materials, and concluded that 3D printed materials are feasible for use in DEM validation studies. These studies have demonstrated the usefulness and potential benefits of 3D printed particle analogs. The objective of the current research is to examine whether the mechanical behavior of natural soils can be reproduced using 3D printed analogs with the aid of a Hertz-based normalization scheme.

HERTZ-BASED NORMALIZATION FRAMEWORK

The current research is focused on the force–displacement response of particles in contact within the micro-asperities yielding and Hertzian behavior range (i.e. stages I and II in Figure 1); future investigations will address the potential effect of micro-asperity and plastic yielding. The applied boundary stresses that control the contact normal forces between particles were selected to avoid significant yielding and breakage at contacts as shown in Ahmed et al. (2019). Considering the elastic contact behavior described by Hertz contact theory (i.e. stage II in Figure 1), the mechanical property of main interest is the particles' Young's modulus (i.e. normal stiffness).

The average normal force F at particle-particle contacts within a random packing of equal size spheres is related to the applied effective boundary stress σ', the particle radius R and the assembly void ratio, e. This relationship can be expressed as $F = C\sigma' R^2$, where C is a coefficient that depends on void ratio e and is expressed as $C = \pi(1+e)^{2/3}$ (Santamarina 2003). Considering spheres of equal sizes in an assembly of particles with boundary stress σ', Equation 1 can be written as:

$$\delta = \left[\frac{9}{16} \frac{(C\sigma' R^2)^2}{RE^{*2}} \right]^{1/3} \quad (2)$$

For contacts within assemblies of mono-sized spheres with the same void ratio and particle size but composed of particles of different constituent materials (i.e. with different Young's

modulus) to undergo the same deformation (i.e. $\delta_1 = \delta_2$) the following condition must be met:

$$\frac{\sigma'_1}{E^*_1} = \frac{\sigma'_2}{E^*_2} \quad or \quad \frac{F_1}{E^*_1} = \frac{F_2}{E^*_2} \tag{3}$$

This relationship, obtained from Hertz theory, indicates that the same deformation will be experienced at the particle-particle contacts as long as the ratio of the applied boundary stress (or contact force) to material Young's modulus is equal for the two assemblies.

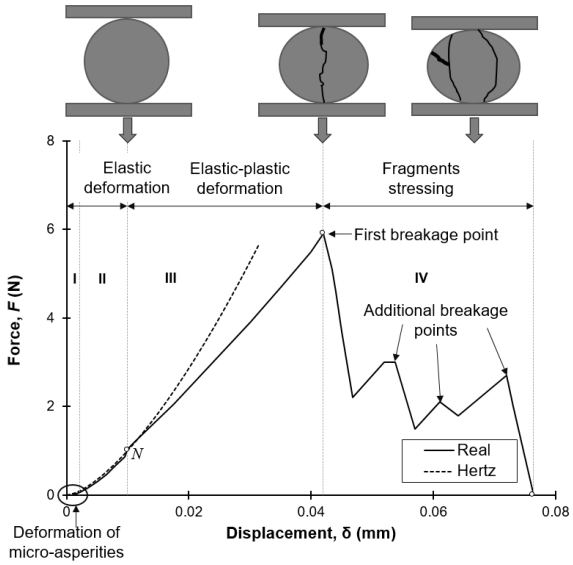

Figure 1. Contact force-displacement curve up to failure (after Antonyuk, et al. 2005)

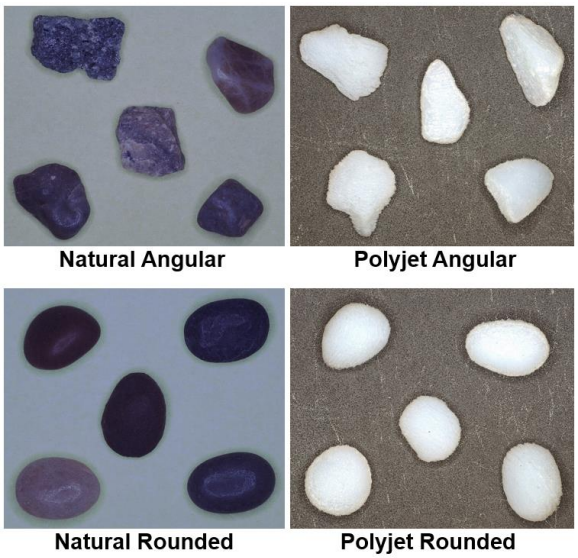

Figure 2. Natural and 3D printed angular and rounded particles

MATERIALS

Natural Quartz: Quartz particles were separated by sieving a natural well-graded sand to obtain samples passing through #6 (3.36 mm) and retained on #8 (2.38 mm) sieves. This results in a poorly-graded sandy soil which is composed of both angular and rounded particles. The particles were then manually separated to create two sands, one angular and one rounded. This

methodology ensures that both natural sands have the same gradation and mineralogy. Figure 2 shows sample angular and rounded particles that are used in this study.

3D Printed Analogs: 90 angular and 70 rounded natural sand particles were chosen randomly for scanning. The particles were scanned using an X-ray CT scanner with a resolution of 10 μm. 3D scans such as those shown in Figure 3 are used to print the 3D printed analogs. Polyjet technology similar to that described in Adamidis et al. (2019) was used to generate the analogs. Pictures of some of the printed angular and rounded particles are shown in Figure 2.

Comparison of Shape Parameters: The particle shape parameters that are generally used to distinguish angular and rounded particles are roundness and sphericity. Roundness is the measure of the sharpness of a particle's edges and corners, whereas sphericity is the measure of degree to which the particle resembles to a spherical shape. In the current study, particle shape parameters (roundness and sphericity) were obtained from image analysis of pictures of particles using the code presented by Zheng and Hryciw (2015). Figure 4 shows the comparison of shape parameters obtained for both natural and 3D printed particles. As shown, the shape parameters of the 3D printed particles compare well with those of the natural particles.

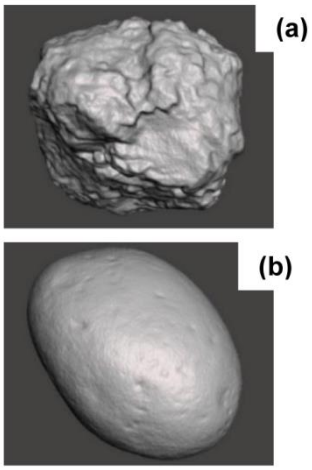

Figure 3. 3D scans of (a) angular, and (b) rounded particles

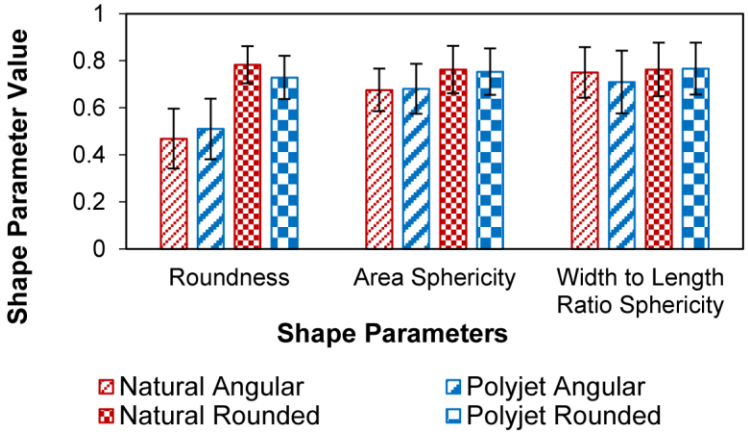

Figure 4. Comparison of shape parameters between natural particles and 3D printed analogs (parameters described in Zheng and Hryciw 2015).

EXPERIMENTAL METHODS

1D Compression Test: A schematic of the 1D compression testing setup is shown in Figure 5. A custom-made compression mold made of 316 stainless steel with an inside diameter and height of 63.5 mm contains the specimen. A digital load actuator is used to apply strain-controlled compression to the specimen during testing. Displacement is measured with a linear variable differential transformer (LVDT) and the applied load is measured with a load cell.

Specimens of natural sand and 3D printed analogs were tested, as shown in Table 1. The specimens were prepared by pouring the particles in the testing mold in three lifts. The side of the specimen was tapped with a rubber mallet to densify it to its target void ratio. Specimens of each material were prepared at an initial void ratio of 0.55±0.02.

Table 1. Properties of materials used in the experiments

Material	Young's modulus, E (GPa)	Poisson's ratio, ν	Specific gravity, G_s
Natural Quartz Sand Particles	76[1]	0.31[2]	2.65[3]
3D Printed Particles	2.4[4]	0.3[5]	1.18[6]

[1, 2, 3]Santamarina et al. (2001); [4]Material specification sheet; [5]Assumed; [6]Measured in lab

The maximum normal stress applied to the specimens was selected carefully to prevent breakage or significant yielding of the particles according to Ahmed et al. (2019). The authors conducted particle-particle compression test on 3D printed spheres and observed no crushing at the levels of contact forces which particles are expected to experience at the applied boundary stresses. However, some level of plastic yielding likely took place.

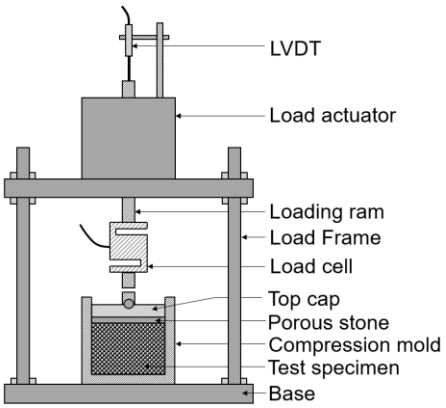

Figure 5. 1D compression test setup

Bender Element Test: The shear wave velocity in both natural sand and 3D printed analogs were measured using bender elements. A schematic of the bender element test setup is shown in Figure 6. The specimen height and diameter were approximately 100 mm and 70 mm, respectively contained in a latex membrane. Both top and bottom cap have one bender element attached. Each bender element is 12.7 mm in length, 8 mm in width, and 0.66 mm in thickness. Isotropic confining pressure was applied using a vacuum pump. A pair of bender elements was used to send and receive the *S*-waves. The shear wave velocity was calculated from the time to travel from transmitter bender to receiver bender, and distance between two benders. The arrival time was taken as the initial rise of the signal wave, where initial rise was defined as the time

when a signal first crossed the X-axis (i.e. from a negative to positive voltage). Shear wave velocities were obtained for specimens with initial target void ratios similar to those in 1D compression tests (0.55±0.02). The specimens were prepared following the same procedure as stated above. The minimum and maximum isotropic stresses applied were 10 kPa and 70 kPa, respectively.

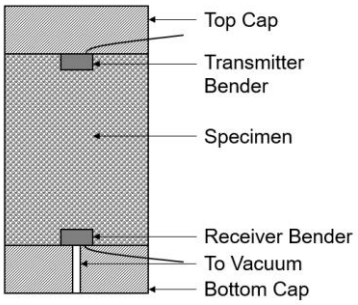

Figure 6. Bender element test setup

TEST RESULTS AND DISCUSSION

1D Compression Test: Figures 7 and 8 present the results of 1D compression tests in terms of change in void ratio (Δe) versus applied vertical stress (σ'_v) for specimens composed of rounded and angular particles (both natural and 3D printed). As shown in Figures 7a and 8a, the specimens of 3D printed analogs require lower stress to achieve a certain change in void ratio. In normalized stress space (σ'_v/E^*), the compression response aggregates to a tighter band (Figures 7b and 8b) showing that the normalization scheme accounts for some of the differences in response. However, the curves for 3D printed particles in normalized space lie to the right of curves for natural particles. It is also noted that the 3D printed particles are more compressible than the natural ones as observed from Figures 7 and 8.

The experimental results for specimens with different Young's modulus indicate that the proposed framework does not completely normalize the effect of particle stiffness. This is because the proposed framework does not address other effects that influence the compression behavior of granular assemblies, such as yielding of micro-asperities at contacts and particle rearrangement and resulting fabric changes. Figures 7c and 8c show the experimental results using a different normalization scheme, one that normalizes the applied stress by the Young's modulus raised to an empirically determined power $n = 0.70$ as:

$$\frac{\sigma'_{v1}}{E^{*n}_1} = \frac{\sigma'_{v2}}{E^{*n}_2} \tag{4}$$

As shown, the compression curves collapse to a tighter band, indicating that a power normalization better captures effects than the purely analytical scheme (Equation 3). Such effects are likely to be related to rearrangement of particles, as previously described, to plastic deformations of micro-asperities at small loads, and possibly yielding at a small number of contacts due to concentration of forces, as shown by Discrete Element Modeling (DEM) simulations by authors such as Barreto (2009) and Ahmed et al. (2019).

Bender Element Test

Shear wave velocity: The shear wave velocities for both angular and rounded natural and 3D printed particles are estimated by using bender elements. The corresponding shear moduli or

small-strain moduli are then determined using the relationship $G_{max} = \rho V_s^2$, where ρ is the density of the soil specimen.

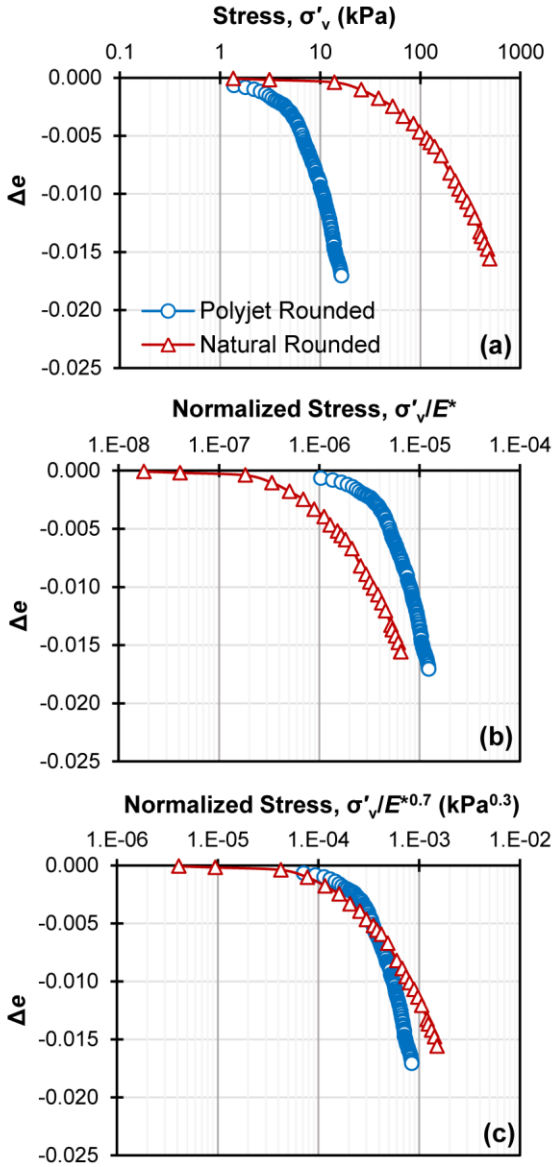

Figure 7. 1D compression test results for rounded particles: (a) Δ*e* vs. stress, (b) Δ*e* vs. normalized stress (σ'_v/E^*), and (c) Δ*e* vs. normalized stress ($\sigma'_v/E^{*0.7}$) plots

The estimated shear wave velocities for all the specimens are shown in Figure 9 for specimens with a void ratio of 0.55±0.02. The 3D printed particle specimens exhibit higher shear wave velocities compared to the natural particle specimens. Although the shape and size of 3D printed particles are kept similar to those of natural particles, the likely cause of higher shear wave velocity in 3D printed particles is the higher contact area that is facilitated by the softer polymer material as compared to the quartz, in agreement with Santamarina (2003). The rounded particle specimens exhibit slightly higher shear wave velocities than the angular particles for both natural and 3D printed specimens which is consistent with literature (e.g. Cho et al. 2006).

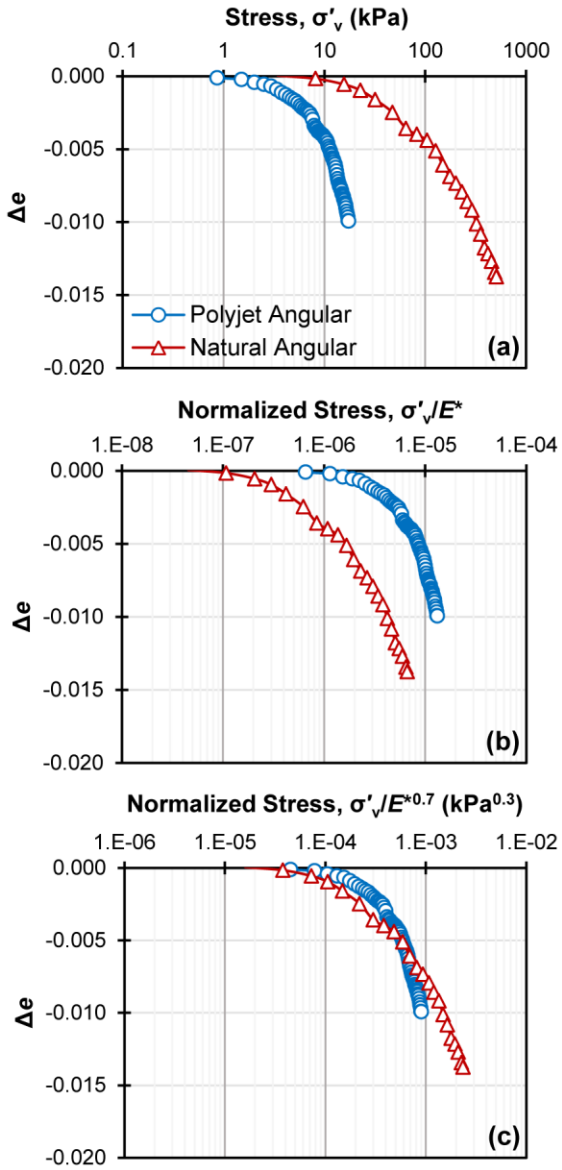

Figure 8. 1D compression test results for angular particles: (a) Δ*e* vs. stress, (b) Δ*e* vs. normalized stress (σ'_v/E^*), and (c) Δ*e* vs. normalized stress ($\sigma'_v/E^{*0.7}$) plots

Shear modulus: Figure 10 shows the small-strain moduli estimated for all the specimens with a void ratio of 0.55±0.02. The natural particle specimens exhibit higher shear moduli compared to the 3D printed particle specimens due to the sand specimens' greater density. Also, for both 3D printed and natural specimens, the rounded particle specimens demonstrate higher shear moduli.

The shear modulus of a particle assembly under an isotropic stress, σ′, can be represented by a power relationship $G_{max} = AF(e)\sigma'^{n}$ (e.g. Hardin and Richart 1963), where *A* is dependent on the particle constituent materials' Young's modulus and Poisson's ratio, *F*(e) is dependent on the assembly void ratio, and *n* is dependent on particle shape. These parameters can be determined empirically or analytically for an isotropic fabric assembly under isotropic stress condition using Hertz contact theory (e.g. Yimsiri and Soga 2000).

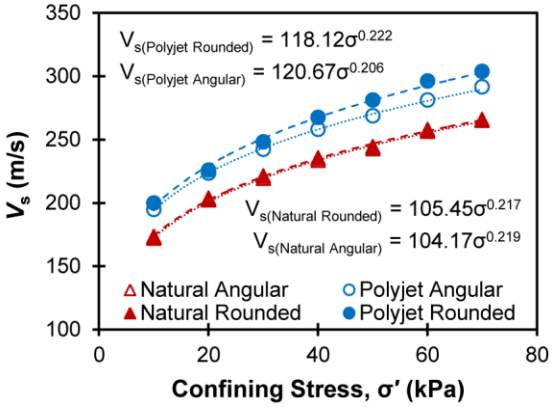

Figure 9. Shear wave velocities (V_s) for angular and rounded natural and 3D printed particles

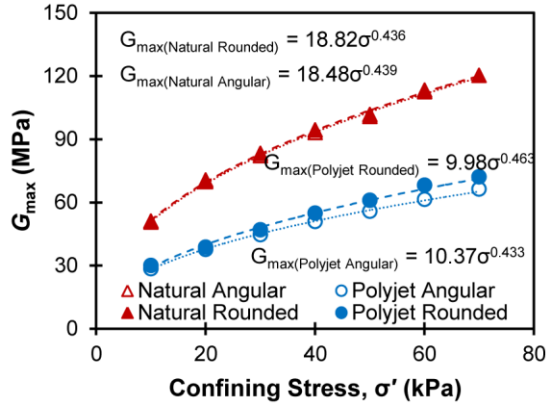

Figure 10. Shear moduli (G_{max}) for angular and rounded natural and 3D printed particles

The empirically fitted relationships for G_{max} using equation 5 are also shown in Figure 10. Since the initial void ratio for all the specimens is 0.55±0.02, the F(e) values are similar, and the obtained A values are larger for natural particles compared to those for 3D printed particles due to the higher Young's modulus of natural particles. Also, the values of exponent n obtained from the fitted equations ranges between 0.433 and 0.463 for both materials, which are consistent with literature (e.g. Hardin and Black 1966).

CONCLUSION

This paper presents a study on the feasibility of 3D printed soil analogs to model the coarse grained soil behavior. A representative number of angular and rounded natural sand particles was scanned using X-ray CT scanner and printed using a 3D printer. A comparative study of shape parameters (i.e. roundness and sphericity) for natural and 3D printed particles demonstrates the capability of 3D printers to reproduce 3D printed analogs of similar shape and size to those of natural particles. The 1D compression stress–strain response of both natural particles and 3D printed analogs collapses to a tight band if an empirical exponent is introduced in the Hertz-based normalization for equivalent contact deformation. The small-strain moduli–mean effective stress relationship for both natural particles and 3D printed analogs are in agreement to those reported in the existing literature; however, the shear wave velocity of the 3DP analogs is larger than that of the natural sand. This research provides evidence that the proposed normalization

scheme can be used to model aspects of the mechanical behavior of coarse-grained soils using 3D printed particle analogs.

ACKNOWLEDGEMENTS

This material is based upon work supported in part by the National Science Foundation (NSF) under award No. 1735732. Any opinions, findings and conclusions or recommendations expressed in this material are those of the author(s) and do not necessarily reflect those of the NSF.

REFERENCES

Adamidis, O., Alber, S., and Anastasopoulos, I. (2019). "Assessment of Three-Dimensional Printing of Granular Media for Geotechnical Applications." *Geotechnical Testing Journal*, 43(3). DOI: 10.1520/GTJ20180259.

Ahmed, S. S., Singh, M., and Martinez, A. (2019). "Particle-Scale Contact Response of 3D Printed Particle Analogs." Presented in *Engineering Mechanics Institute Conference*, Caltech, 18-21 June 2019.

Antonyuk, S., Tomas, J., Heinrich, S., and Mörl, L. (2005). "Breakage behaviour of spherical granulates by compression." *Chemical Engineering Science*, 60(14), 4031-4044.

Athanassiadis, A.G., Miskin, M.Z., Kaplan, P., Rodenberg, N., Lee, S.H., Merritt, J., Brown, E., Amend, J., Lipson, H., and Jaeger, H.M. (2014). "Particle shape effects on the stress response of granular packings." *Soft Matter*, 10(1), 48-59.

Barreto Gonzalez, D. (2009). *Numerical and experimental investigation into the behaviour of granular materials under generalized stress states*. PhD thesis, Department of Civil and Environmental Engineering, Imperial College London.

Cavarretta, I., Coop, M., and O'Sullivan, C. (2010). "The influence of particle characteristics on the behaviour of coarse grained soils." *Géotechnique*, 60(6), 413-423.

Cho, G. C., Dodds, J., and Santamarina, J. C. (2006). "Particle shape effects on packing density, stiffness, and strength: natural and crushed sands." *Journal of Geotechnical and Geoenvironmental Engineering*, 132(5), 591-602.

Cole, D. M., and Peters, J.F. (2007). "A physically based approach to granular media mechanics: grain-scale experiments, initial results and implications to numerical modeling." *Granular Matter*, 9(5), 309-321.

Greenwood, J.A., and Tripp, J.H. (1967). "The elastic contact of rough spheres." *Journal of Applied Mechanics*, 34(1), 153-159.

Gupta, R., Salager, S., Wang, K., and Sun, W. (2018). "Open-source support toward validating and falsifying discrete mechanics models using synthetic granular materials—Part I: Experimental tests with particles manufactured by a 3D printer." *Acta Geotechnica*, 15 p.

Hanaor, A. H., Gan, Y., Revay, M., Airey, D. W., and Einav, I. (2016). "3D printable geomaterials." *Géotechnique*, 66(4), 323-332.

Hardin, B. O., and Black, W. L. (1966). "Sand stiffness under various triaxial stresses." *J. Soil Mech. Found. Engng.*, ASCE. 92(2), 27-42.

Hardin, B. O., and Richart, F. E. (1963). "Elastic wave velocities in granular soils." *J. Soil Mech. Found. Engng*., ASCE. 89, SM1, 39-56.

Jiménez, M., Romero, L., Domínguez, I. A., Espinosa, M. D. M., and Domínguez, M. (2019). "Additive manufacturing technologies: An overview about 3D printing methods and future prospects." *Complexity*, DOI: 10.1155/2019/9656938.

Kittu, A., Watters, M., Cavarretta, I., and Bernhardt-Barry, M. L. (2019). "Characterization of additive manufactured particles for DEM validation studies." *Granular Matter*, 21(3), 65.
Matsumura, S., Kobayashi, T., Mizutani, T., and Bathurst, R. J. (2017). "Manufacture of Bonded Granular Soil Using X-Ray CT Scanning and 3D Printing." *Geotechnical Testing Journal*, 40(6), 1000-1010.
Miskin, M. Z., and Jaeger, H. M. (2013). "Adapting granular materials through artificial evolution." *Nature Materials*, 12(4), 326-331.
Nadimi, S., and Fonseca, J. (2017). "Single-grain virtualization for contact behavior analysis on sand." *Journal of Geotechnical and Geoenvironmental Engineering*, 143(9), 06017010.
Santamarina, J. C. (2003). "Soil behavior at the microscale: Particle forces." *Proc., Soil Behavior and Soft Ground Construction*, GSP No. 119, ASCE, Reston, VA, 25-56.
Santamarina, J. C., Klein, A., and Fam, M. A. (2001). *Soils and waves: Particulate materials behavior, characterization and process monitoring*. Wiley & Sons, 508 p.
Senetakis, K., Coop, M. R., and Todisco, M. C. (2013). "Tangential load–deflection behaviour at the contacts of soil particles." *Géotechnique Letters*, 3(2), 59-66.
Tofail, S. A., Koumoulos, E. P., Bandyopadhyay, A., Bose, S., O'Donoghue, L., and Charitidis, C. (2018). "Additive manufacturing: scientific and technological challenges, market uptake and opportunities." *Materials Today*, 21(1), 22-37.
Yimsiri, S., and Soga, K. (2000). "Micromechanics-based stress–strain behaviour of soils at small strains." *Géotechnique*, 50(5), 559-571.
Zhao, B., Wang, J., Coop, M. R., Viggiani, G., and Jiang, M. (2015). "An investigation of single sand particle fracture using X-ray micro-tomography." *Géotechnique*, 65(8), 625-641.
Zheng, J., and Hryciw, R. D. (2015). "Traditional soil particle sphericity, roundness and surface roughness by computational geometry." *Géotechnique*, 65(6), 494-506.